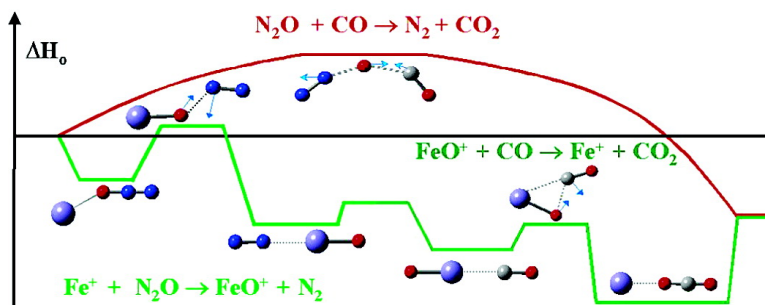


## O-Atom Transport Catalysis by Atomic Cations in the Gas Phase: Reduction of NO by CO

Voislav Blagojevic, Galina Orlova, and Diethard K. Bohme

*J. Am. Chem. Soc.*, **2005**, 127 (10), 3545-3555 • DOI: 10.1021/ja044950m • Publication Date (Web): 22 February 2005

Downloaded from <http://pubs.acs.org> on March 24, 2009



### More About This Article

Additional resources and features associated with this article are available within the HTML version:

- Supporting Information
- Links to the 6 articles that cite this article, as of the time of this article download
- Access to high resolution figures
- Links to articles and content related to this article
- Copyright permission to reproduce figures and/or text from this article

[View the Full Text HTML](#)

## O-Atom Transport Catalysis by Atomic Cations in the Gas Phase: Reduction of N<sub>2</sub>O by CO

Voislav Blagojevic, Galina Orlova, and Diethard K. Bohme\*

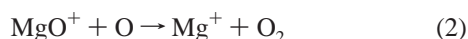
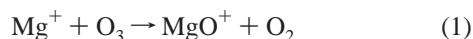
Contribution from the Department of Chemistry, Centre for Research in Mass Spectrometry and Centre for Research in Earth and Space Science, York University, Toronto, Ontario, Canada, M3J 1P3

Received August 20, 2004; E-mail: dkbohme@yorku.ca

**Abstract:** Atomic cations (26), M<sup>+</sup>, have been shown to lie within a thermodynamic window for O-atom transport catalysis of the reduction of N<sub>2</sub>O by CO and have been checked for catalytic activity at room temperature with kinetic measurements using an inductively-coupled plasma/selected-ion flow tube (ICP/SIFT) tandem mass spectrometer. Only 10 of these 26 atomic cations were seen to be catalytic: Ca<sup>+</sup>, Fe<sup>+</sup>, Ge<sup>+</sup>, Sr<sup>+</sup>, Ba<sup>+</sup>, Os<sup>+</sup>, Ir<sup>+</sup>, Pt<sup>+</sup>, Eu<sup>+</sup>, and Yb<sup>+</sup>. The remaining 16 cations that lie in the thermodynamic window (Cr<sup>+</sup>, Mn<sup>+</sup>, Co<sup>+</sup>, Ni<sup>+</sup>, Cu<sup>+</sup>, Se<sup>+</sup>, Mo<sup>+</sup>, Ru<sup>+</sup>, Rh<sup>+</sup>, Sn<sup>+</sup>, Te<sup>+</sup>, Re<sup>+</sup>, Pb<sup>+</sup>, Bi<sup>+</sup>, Tm<sup>+</sup>, and Lu<sup>+</sup>) react too slowly at room temperature either in the formation of MO<sup>+</sup> or in its reduction by CO. Many of these reactions are known to be spin forbidden and a few actually may lie outside the thermodynamic window. A new measure of efficiency is introduced for catalytic cycles that allows the discrimination between catalytic cations on the basis of the efficiencies of the two legs of the catalytic cycle. Also, a potential-energy landscape is computed for the reduction of N<sub>2</sub>O by CO catalyzed by Fe<sup>+</sup>(<sup>6</sup>D) that vividly illustrates the operation of an ionic catalyst.

### 1. Introduction

The natural affinity of an atomic cation for an O atom can afford an alternate path for the transfer of an O atom from one molecule to another: the atomic cation simply picks up the O atom from a donor molecule and delivers it to an acceptor molecule (and in the process is regenerated). Furthermore, the extra dimension of charge brought to bear in this chemical transformation leads to a significant increase in the rate of both the O-atom pickup and the O-atom delivery: the overall O-atom transfer is catalyzed as well. The increase in these rates is a consequence of the electrostatic attraction between ions and molecules that acts to reduce kinetic activation energies. The first example of this "O-atom transport catalysis" of which we are aware, although not recognized as such at the time, is the reaction couple (eq 1) and (eq 2) reported in 1968 in the context of the chemistry of the earth's ionosphere (the E-region):<sup>1a</sup>



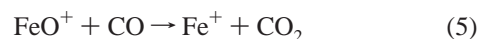
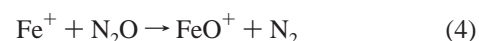
Both of these reactions are fast at 300 K,  $k_1 = 2.3 \times 10^{-10}$  and  $k_2 = 1 \times 10^{-10}$  cm<sup>3</sup> molecule<sup>-1</sup> s<sup>-1</sup>, as measured with the early flowing afterglow technique.<sup>1a</sup> Overall, the Mg<sup>+</sup> cations act to catalyze the reduction of ozone by atomic oxygen, reaction 3,

which proceeds with a rate coefficient  $k = 9.1 \times 10^{-15}$  cm<sup>3</sup> molecule<sup>-1</sup> s<sup>-1</sup> at room temperature ( $E_a = 4.4$  kcal mol<sup>-1</sup>).<sup>1b</sup>



Of atmospheric interest at the time was that reaction 2 keeps Mg<sup>+</sup>/MgO<sup>+</sup> large in the E region (where MgO<sup>+</sup> can be lost by recombination with electrons) and not that reactions 1 and 2 constitute a catalytic cycle for the reduction of O<sub>3</sub> by O.

The landmark experiments of Kappes and Staley in 1981 demonstrated the first cyclic reduction of N<sub>2</sub>O by CO in the gas phase in the presence of atomic metal cations.<sup>2</sup> These authors reported the occurrence, in an ion-cyclotron resonance (ICR) spectrometer, of reactions 4 and 5 in which the Fe<sup>+</sup> cation acts as a catalyst for the overall transformation given by reaction 6.

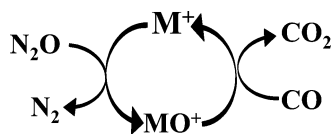


The reported rate coefficients were  $k_4 = 7 \times 10^{-11}$  and  $k_5 = 9 \times 10^{-10}$  cm<sup>3</sup> molecule<sup>-1</sup> s<sup>-1</sup>. Five other transition-metal cations, Ti<sup>+</sup>, Zr<sup>+</sup>, V<sup>+</sup>, Nb<sup>+</sup>, and Cr<sup>+</sup>, were tried but were found not to act as catalysts in that the oxides of these metal cations were observed not to be reduced by CO with a measurable rate. Selected-ion flow tube (SIFT) experiments in 1995 provided somewhat lower rate coefficients for  $k_4 = 3.1 \times 10^{-11}$  and  $k_5$

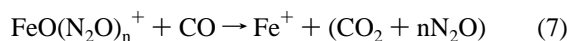
(1) (a) Ferguson, E. E.; Fehsenfeld, F. C. *J. Geophys. Res.* **1968**, *73*, 6215–6223. (b) Kaufman, F. *Defense Nuclear Agency Reaction Rate Handbook*, 2nd ed.; DASIAC, General Electric, TEMPO: Santa Barbara, California, 1972; Chapter 19.

(2) Kappes, M. M.; Staley, R. H. *J. Am. Chem. Soc.* **1981**, *103*, 1286.

Scheme 1



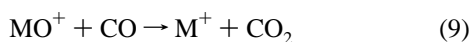
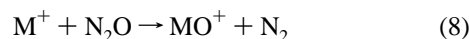
$= 2.05 \times 10^{-10} \text{ cm}^3 \text{ molecule}^{-1} \text{ s}^{-1}$  at room temperature and also demonstrated that the catalytic cycle is not poisoned by  $\text{N}_2\text{O}$ , since  $\text{FeO}(\text{N}_2\text{O})_n^+$  remains reactive at least up to  $n = 3$  according to reaction 7.<sup>3</sup>



More recently  $\text{Pt}^+$  has been shown to undergo reactions of type 4 and 5 with  $k = 7 \times 10^{-11}$  and  $k = 6.7 \times 10^{-10} \text{ cm}^3 \text{ molecule}^{-1} \text{ s}^{-1}$ , respectively, which means that  $\text{Pt}^+$  can catalyze reaction 6 as well.<sup>4</sup> In our laboratory, using ICP-SIFT tandem mass spectrometry, we have recently confirmed the catalytic activity of  $\text{Fe}^+$ , were able to add  $\text{Os}^+$  and  $\text{Ir}^+$  to the list of catalysts active in the reduction of  $\text{N}_2\text{O}$  by  $\text{CO}$ , and extended observations of atomic metal-cation catalysis to the reduction of  $\text{NO}_2$  and  $\text{NO}$  by  $\text{CO}$ .<sup>5a</sup> Very recently platinum cluster cations,  $\text{Pt}_n^+$  ( $n = 6-8$ ), also have been observed to catalyze reaction 6.<sup>5b</sup>

Here we ask whether the four atomic ions,  $\text{Fe}^+$ ,  $\text{Pt}^+$ ,  $\text{Os}^+$ , and  $\text{Ir}^+$ , represent a complete set of atomic cations effective as catalysts in the reduction of  $\text{N}_2\text{O}$  by  $\text{CO}$  and if not, why not? In answering these questions, we formulate a general thermodynamic requirement for this catalysis and extend the kinetic measurements to 22 other atomic cations that meet this requirement. The 22 atomic cations are chosen from the first-row atomic cations from  $\text{K}^+$  to  $\text{Se}^+$ , the second-row atomic cations from  $\text{Rb}^+$  to  $\text{Te}^+$  (excluding  $\text{Tc}^+$ ) and the third-row atomic cations from  $\text{Cs}^+$  to  $\text{Bi}^+$ , as well as the lanthanide cations (excluding  $\text{Pm}^+$ ).

Since the reduction of  $\text{N}_2\text{O}$  by  $\text{CO}$  involves the transfer of an O atom from  $\text{N}_2\text{O}$  to  $\text{CO}$ , an atomic metal cation  $\text{M}^+$  must have an O-atom affinity that lies between  $\text{OA}(\text{N}_2)$  and  $\text{OA}(\text{CO})$  to have the thermodynamic potential to catalyze reaction 6. Available O-atom affinities<sup>6</sup> indicate a thermodynamic “window” of  $87 \text{ kcal mol}^{-1}$ ,  $40 \text{ kcal mol}^{-1} < \text{OA}(\text{M}^+) < 127 \text{ kcal mol}^{-1}$ , and that 26 of the 59 first, second, third row and lanthanide cations that we have investigated meet, within the uncertainties of the known O-atom affinities, the thermodynamic criterion for the catalytic reduction of  $\text{N}_2\text{O}$  by  $\text{CO}$  according to reactions 8 and 9 and illustrated in Scheme 1.



However, we will show that less than half of these 26 cations have the required kinetic properties to exhibit this catalysis to a measurable extent. Furthermore, the versatility of the ICP-

SIFT tandem mass spectrometer used in these experiments has provided a means to track the steady-state achieved in these catalytic cycles. Also, we were able to explore the action of higher oxide cations as catalysts and the influence of  $\text{N}_2\text{O}$  ligation on the catalytic activity of atomic ions.

## 2. Methods Section

**2.1. Experimental Methods.** The reactions were investigated in an inductively-coupled plasma/selected-ion flow tube (ICP/SIFT) tandem mass spectrometer. The apparatus has been described previously.<sup>7</sup> Elemental cations of interest are generated in an argon plasma operating at atmospheric pressure and ca. 5500 K fed with a dilute solution of salts containing the corresponding element. The ions are introduced into a differentially pumped sampling interface, then mass selected by a quadrupole mass filter, and injected into a flow tube flushed with He buffer gas at 0.35 Torr and  $295 \pm 2 \text{ K}$ . The metal ions cool by radiation and collision with argon and helium from their point of origin in the ICP to the entrance of the reaction region. The state distribution of the ICP ions and their relaxation by collision and radiation before they reach the reaction region have been discussed in detail previously.<sup>8</sup> Neutral reagent molecules were added downstream into the reaction region. Ions present in the reacting mixtures were sampled by a second quadrupole mass spectrometer.

In our previous studies of reactions of atomic metal cations with  $\text{N}_2\text{O}$ ,<sup>8</sup> the  $\text{N}_2\text{O}$  was added directly into the reaction region downstream in the flow tube. Rate coefficients for the oxidation reactions of  $\text{M}^+$  were derived from the linear semilogarithmic decays of  $\text{M}^+$  in the usual way using pseudo first-order kinetics.<sup>7-9</sup> In the studies reported here of atomic-oxide cation chemistry with  $\text{CO}$ , the atomic-oxide cation was produced upstream from the reaction of the atomic ion with  $\text{N}_2\text{O}$ , and  $\text{CO}$  was introduced into the reaction region further downstream. Due to the presence of  $\text{N}_2\text{O}$  in the reaction region, a steady state was established between the oxidation reaction of  $\text{M}^+$  with  $\text{N}_2\text{O}$  and the reduction reaction of  $\text{MO}^+$  with  $\text{CO}$ . Only lower limits to the rate coefficients could be obtained for the reduction reactions from the initial tangent to the curved semilogarithmic decays of  $\text{MO}^+$ . To obtain absolute values for the rate coefficients of the reduction reactions we took advantage of the establishment of a steady state and used the steady-state analysis described in the text to derive the rate coefficient for the reduction reaction.

All measurements were performed at room temperature of  $295 \pm 2 \text{ K}$  and at a helium operating pressure of  $0.35 \pm 0.01 \text{ Torr}$ . The nitrous oxide was obtained commercially and was of high purity (Matheson Gas products, >98.0%). The carbon monoxide was of C. P. Grade (99.5%) and obtained from Canadian Liquid Air Ltd.

**2.2. Computational Methods.** We have performed a density functional theory (DFT) study of the reactions  $\text{N}_2\text{O} + \text{CO} \rightarrow \text{CO}_2 + \text{N}_2$  (closed singlet) and  $\text{Fe}^+ + \text{N}_2\text{O} \rightarrow \text{MO}^+ + \text{N}_2$  and  $\text{FeO}^+ + \text{CO} \rightarrow \text{Fe}^+ + \text{CO}_2$  (sextet electronic state). All theoretical predictions were made using the Gaussian98 program suite<sup>10</sup> with the hybrid B3LYP<sup>11,12</sup>

(3) Baranov, V.; Javahery, G.; Hopkinson, A. C.; Bohme, D. K. *J. Am. Chem. Soc.* **1995**, *117*, 12801.

(4) Brönstrup, M.; Schröder, D.; Kretzschmar, I.; Schwarz, H.; Harvey, J. N. *J. Am. Chem. Soc.* **2001**, *123*, 142.

(5) (a) Blagojevic, V.; Jarvis, M. J. Y.; Flaim, E.; Koyanagi, G. K.; Lavrov, V. V.; Bohme, D. K. *Angew. Chem.* **2003**, *115*, 5053; *Angew. Chem., Int. Ed.* **2003**, *42*, 4923. (b) Balaj, O. P.; Balteanu, I.; Rossteuscher, T. T. J.; Beyer, M. K.; Bondybey, V. E. *Angew. Chem.* **2004**, *116*, 6681; *Angew. Chem., Int. Ed.* **2004**, *47*, 6519.

(6) Lias, S. G.; Bartmess, J. E.; Liebman, J. F.; Holmes, J. L.; Levin, R. D.; Mallard, W. G. *J. Phys. Chem. Ref. Data* **1988**, *17* (Suppl 1).

(7) Koyanagi, G. K.; Lavrov, V. V.; Baranov, V. I.; Bandura, D.; Tanner, S. D.; McLaren, J. W.; Bohme, D. K. *Int. J. Mass Spectrom.* **2000**, *194*, L1.

(8) Lavrov, V. V.; Blagojevic, V.; Koyanagi, G. K.; Orlova, G.; Bohme, D. K. *J. Phys. Chem. A* **2004**, *108*, 5610.

(9) (a) Mackay, G. I.; Vlachos, G. D.; Bohme, D. K.; Schiff, H. I. *Int. J. Mass Spectrom. Ion Phys.* **1980**, *36*, 259. (b) Raksit, A. B.; Bohme, D. K. *Int. J. Mass Spectrom. Ion Processes* **1983**, *55*, 69.

(10) Frisch, M. J.; Trucks, G. W.; Schlegel, H. B.; Scuseria, G. E.; Robb, M. A.; Cheeseman, J. R.; Zakrzewski, V. G.; Montgomery, J. A., Jr.; Stratmann, R. E.; Burant, J. C.; Dapprich, S.; Millam, J. M.; Daniels, A. D.; Kudin, K. N.; Strain, M. C.; Farkas, O.; Tomasi, J.; Barone, V.; Cossi, M.; Cammi, R.; Mennucci, B.; Pomelli, C.; Adamo, C.; Clifford, S.; Ochterski, J.; Petersson, G. A.; Ayala, P. Y.; Cui, Q.; Morokuma, K.; Malick, D. K.; Rabuck, A. D.; Raghavachari, K.; Foresman, J. B.; Cioslowski, J.; Ortiz, J. V.; Stefanov, B. B.; Liu, G.; Liashenko, A.; Piskorz, P.; Komaromi, I.; Gomperts, R.; Martin, R. L.; Fox, D. J.; Keith, T.; Al-Laham, M. A.; Peng, C. Y.; Nanayakkara, A.; Gonzalez, C.; Challacombe, M.; Gill, P. M. W.; Johnson, B. G.; Chen, W.; Wong, M. W.; Andres, J. L.; Head-Gordon, M.; Replogle, E. S.; Pople, J. A. *Gaussian 98*, revision A.11; Gaussian, Inc.: Pittsburgh, PA, 1998.

**Table 1.** Rate Coefficients for Reactions of Atomic-metal Cations  $M^+$  with  $N_2O$  and of Metal-Monoxide Cations  $MO^+$  with  $CO$  Measured at Room Temperature Using an ICP/SIFT Tandem Mass Spectrometer<sup>a</sup>

$M^+$	OA( $M^+$ ) <sup>b</sup>	$M^+ + N_2O$		$MO^+ + CO$		$k^d$
		$k^c$	products	$k^c$	products	
Ca <sup>+</sup>	77.2	$1.6 \times 10^{-10}$	CaO <sup>+</sup>	$\geq 5.7 \times 10^{-12}$	Ca <sup>+</sup>	$2.5 \times 10^{-10}$
Cr <sup>+</sup>	$85.8 \pm 2.8$	$1.5 \times 10^{-13}$	CrO <sup>+</sup> (0.98) Cr <sup>+</sup> ·N <sub>2</sub> O (0.02)	$< 10^{-13}$		
Mn <sup>+</sup>	$68.0 \pm 3.0$	$< 10^{-13}$	Mn <sup>+</sup> ·N <sub>2</sub> O	NA		
Fe <sup>+</sup>	$80.0 \pm 1.4$	$3.7 \times 10^{-11}$	FeO <sup>+</sup>	$\geq 2.4 \times 10^{-10c}$	Fe <sup>+</sup>	$1.8 \times 10^{-10}$
Co <sup>+</sup>	$74.9 \pm 1.2$	$2.1 \times 10^{-12}$	CoO <sup>+</sup> (0.50) Co <sup>+</sup> ·N <sub>2</sub> O (0.50)	$< 10^{-13}$		
Ni <sup>+</sup>	$63.2 \pm 1.2$	$6.5 \times 10^{-13}$	Ni <sup>+</sup> ·N <sub>2</sub> O	NA		
Cu <sup>+</sup>	$37.4 \pm 3.5$	$5.7 \times 10^{-13}$	Cu <sup>+</sup> ·N <sub>2</sub> O	NA		
Ge <sup>+</sup>	81.8	$3.6 \times 10^{-10}$	GeO <sup>+</sup>	$\geq 1.1 \times 10^{-10}$	Ge <sup>+</sup>	$2.1 \times 10^{-10}$
Se <sup>+</sup>	92	$1.8 \times 10^{-12}$	SeO <sup>+</sup>	NA		
Sr <sup>+</sup>	71.4	$6.3 \times 10^{-11}$	SrO <sup>+</sup>	$\geq 8.7 \times 10^{-10}$	Sr <sup>+</sup>	$1.0 \times 10^{-10}$
Mo <sup>+</sup>	$116.7 \pm 0.5$	$3.4 \times 10^{-13}$	Mo <sup>+</sup> ·N <sub>2</sub> O	NA		
Ru <sup>+</sup>	$87.9 \pm 1.2$	$3.3 \times 10^{-13}$	Ru <sup>+</sup> ·N <sub>2</sub> O	NA		
Rh <sup>+</sup>	$69.6 \pm 1.4$	$4.0 \times 10^{-13}$	Rh <sup>+</sup> ·N <sub>2</sub> O	NA		
Sn <sup>+</sup>	75.1	$1.0 \times 10^{-13}$	Sn <sup>+</sup> ·N <sub>2</sub> O	NA		
Te <sup>+</sup>	96.6	$< 10^{-13}$	none	NA		
Ba <sup>+</sup>	92.8	$2.4 \times 10^{-10}$	BaO <sup>+</sup>	$\geq 3.1 \times 10^{-11}$	Ba <sup>+</sup>	$2.3 \times 10^{-11}$
Re <sup>+</sup>	$115 \pm 15$	$< 10^{-13}$	ReO <sup>+</sup>	NA		
Os <sup>+</sup>	$100 \pm 12$	$5.8 \times 10^{-10}$	OsO <sup>+</sup> (0.40) OsN <sup>+</sup> (0.60)	$\geq 4.6 \times 10^{-11}$	Os <sup>+</sup>	$\geq 4.0 \times 10^{-13e}$
Ir <sup>+</sup>	59	$2.9 \times 10^{-10}$	IrO <sup>+</sup>	$\geq 2.6 \times 10^{-11}$	Ir <sup>+</sup>	$3.5 \times 10^{-10}$
Pt <sup>+</sup>	77	$1.2 \times 10^{-10}$	PtO <sup>+</sup>	$\geq 1.2 \times 10^{-10}$	Pt <sup>+</sup>	$2.3 \times 10^{-10}$
Pb <sup>+</sup>	53.2	$< 10^{-13}$	Pb <sup>+</sup> ·N <sub>2</sub> O	NA		
Bi <sup>+</sup>	41.6	$< 10^{-13}$	Bi <sup>+</sup> ·N <sub>2</sub> O	NA		
Eu <sup>+</sup>	$93.2 \pm 4.3$	$6.9 \times 10^{-11}$	EuO <sup>+</sup>	$\geq 3.3 \times 10^{-12}$	Eu <sup>+</sup>	NA
Tm <sup>+</sup>	$116.6 \pm 4.3$	$4.4 \times 10^{-12}$	TmO <sup>+</sup>	$< 10^{-13}$		
Yb <sup>+</sup>	$88.1 \pm 5.9$	$6.5 \times 10^{-13}$	YbO <sup>+</sup>	$\geq 1.2 \times 10^{-11}$	Yb <sup>+</sup>	$1.2 \times 10^{-11}$
Lu <sup>+</sup>	$128.0 \pm 4.3$	$2.6 \times 10^{-10}$	LuO <sup>+</sup>	$< 10^{-13}$		

<sup>a</sup> All the metal cations shown are known to have  $OA(N_2) < OA(M^+) < OA(CO)$  within the uncertainties of the known O-atom affinities. <sup>b</sup> OA is the oxygen-atom affinity in kcal mol<sup>-1</sup> (see ref 8 for leading references). <sup>c</sup>  $k$  is the reaction rate coefficient measured in units of cm<sup>3</sup> molecule<sup>-1</sup> s<sup>-1</sup> with an uncertainty less than  $\pm 30\%$ . NA (not available) indicates that the rate coefficient could not be measured because  $MO^+$  could not be established in sufficient amounts. <sup>d</sup> Rate coefficients in units of cm<sup>3</sup> molecule<sup>-1</sup> s<sup>-1</sup> obtained from steady-state analysis (see text). Unless indicated otherwise, the estimated uncertainty is  $\pm 40\%$ . <sup>e</sup> This value is a lower limit because of overlap of OsO<sup>+</sup> with unreactive OsN<sup>+</sup>.

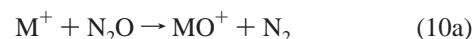
exchange-correlation functional. The triply split 6-311+G(d) basis set<sup>13,14</sup> with one set of diffuse and polarization functions<sup>15,16</sup> was used for all atoms. Harmonic vibrational frequencies were computed to verify minima (all real frequencies) and transition state structures (one imaginary frequency). The connections between transition states and corresponding minima were verified using an intrinsic reaction coordinate technique (IRC) developed by Gonzalez and Schlegel.<sup>17,18</sup> Relative enthalpies at 0 K are reported. Cartesian coordinates and electronic energies for all optimized structures are available as Supporting Information.

### 3. Results and Discussion

**3.1. Thermodynamic Window for O-Atom Transport.** The O-atom affinity of nitrogen to form nitrous oxide,  $OA(N_2)$ , is  $39.95 \pm 0.02$  kcal mol<sup>-1</sup> and that for CO to form CO<sub>2</sub>,  $OA(CO)$ , is  $127.3 \pm 0.02$  kcal mol<sup>-1</sup>.<sup>6</sup> This means that the “thermodynamic window of opportunity” for O-atom transport catalysis of reaction 6 is given by  $40$  kcal mol<sup>-1</sup>  $< OA(M^+) < 127$  kcal mol<sup>-1</sup>.

Of the 59 atomic cations now routinely investigated in our laboratory, 26 fall within this thermodynamic window within the uncertainties of their known O-atom affinities. The known O-atom affinities of these 26 cations are included in Table 1. Two of them,  $OA(Cu^+)$  and  $OA(Lu^+)$ , are borderline.

**3.2. Summary of the Kinetics of Metal-Cation Oxidation Reactions with N<sub>2</sub>O.** Reactions of  $M^+$  with  $N_2O$ , reaction 8, constitute the first leg of the catalytic cycle shown in Scheme 1 and can be measured with the ICP/SIFT tandem mass spectrometer simply by adding  $N_2O$  into the reaction region of the flow tube. This has been done very recently and reported by us for first, second, and third row atomic cations,<sup>8</sup> as well as for lanthanide cations.<sup>19</sup> We found that O-atom transfer was a predominant, although not exclusive, reaction channel. Both N-atom transfer and  $N_2O$  addition were observed to compete with O-atom transfer according to reaction 10.



The measured rate coefficients and product distributions that

- (11) Becke, A. D. *J. Chem. Phys.* **1993**, *98*, 5648.  
 (12) Lee, C.; Yang, W.; Parr, R. G. *Phys. Rev. B* **1988**, *37*, 785.  
 (13) Hehre, W. J.; Ditchfield, R.; Pople, J. A. *J. Chem. Phys.* **1972**, *56*, 2257.  
 (14) Krishnan, R.; Binkley, J. S.; Seeger, R.; Pople, J. A. *J. Chem. Phys.* **1980**, *72*, 650.  
 (15) Chandrasekhar, J.; Andrade, J. G.; Schleyer, P. v. R. *J. Am. Chem. Soc.* **1981**, *103*, 5609.  
 (16) Clark, T.; Chandrasekhar, J.; Spitznagel, G. W.; Schleyer, P. v. R. *J. Comput. Chem.* **1983**, *4*, 294.  
 (17) Gonzalez, C.; Schlegel, H. B. *J. Chem. Phys.* **1989**, *90*, 3154.  
 (18) Gonzalez, C.; Schlegel, H. B. *J. Phys. Chem.* **1990**, *94*, 5523.

- (19) Rowe, B. R.; Viggiano, A. A.; Fehsenfeld, F. C.; Fahey, D. W.; Ferguson, E. E. *J. Chem. Phys.* **1982**, *75*, 742.

we have measured previously<sup>8,19</sup> for the 26 cations within the thermodynamic window for O-atom transport catalysis are given in Table 1. Os<sup>+</sup> is the only cation in this list that exhibits N-atom transfer along with O-atom transfer while Cr<sup>+</sup> and Co<sup>+</sup> show some N<sub>2</sub>O addition. The rates of O-atom transfer exhibit interesting variations: the measured rate coefficients for the 26 cations in question range from <math>10^{-13}</math> to 3 molecule<sup>-1</sup> s<sup>-1</sup>. We have discussed previously that kinetic constraints for these exothermic reactions arise in a number of ways. There may be a genuine activation barrier in the reaction coordinate, as is the case for the reactions with Fe<sup>+</sup> and Rh<sup>+</sup> according to our computations.<sup>8</sup> The reaction may be spin forbidden overall, as is the case with Cr<sup>+</sup>, Mn<sup>+</sup>, Co<sup>+</sup>, Ni<sup>+</sup>, Mo<sup>+</sup>, Ru<sup>+</sup>.<sup>8</sup> In the case of the lanthanide cations (Eu<sup>+</sup>, Tm<sup>+</sup>, Yb<sup>+</sup>, Lu<sup>+</sup>), a barrier to reaction may arise from the energy associated with the promotion of a 4f electron to make two electrons available for bonding.<sup>19</sup> The reaction may be endothermic within the uncertainty of the known oxygen-atom affinity (Cu<sup>+</sup>) or the lowest spin-allowed channel may be endothermic (Co<sup>+</sup>). For the remaining atomic ions that react slowly (as is the case with Se<sup>+</sup>, Sn<sup>+</sup>, Te<sup>+</sup>, Re<sup>+</sup>, Pb<sup>+</sup>, Bi<sup>+</sup>) there is insufficient information available about the energy profile for reaction to provide an explanation for their low O-atom transfer reactivity. Ten atomic ions (Mn<sup>+</sup>, Ni<sup>+</sup>, Cu<sup>+</sup>, Mo<sup>+</sup>, Ru<sup>+</sup>, Rh<sup>+</sup>, Sn<sup>+</sup>, Pb<sup>+</sup>, Bi<sup>+</sup>) simply added N<sub>2</sub>O and Te<sup>+</sup> did not show any products at all under our experimental operating conditions.

Of the 26 cations that lie within the thermodynamic window for O-atom transport catalysis, only 14 (Ca<sup>+</sup>, Cr<sup>+</sup>, Fe<sup>+</sup>, Co<sup>+</sup>, Ge<sup>+</sup>, Sr<sup>+</sup>, Ba<sup>+</sup>, Os<sup>+</sup>, Ir<sup>+</sup>, Pt<sup>+</sup>, Eu<sup>+</sup>, Tm<sup>+</sup>, Yb<sup>+</sup>, and Lu<sup>+</sup>) react sufficiently quickly with N<sub>2</sub>O to establish large enough concentrations of MO<sup>+</sup> to obtain meaningful results for its reaction under our experimental conditions. Two cations (Se<sup>+</sup>, Re<sup>+</sup>) produce insufficient amounts of the oxide cation.

Higher-order addition reactions with N<sub>2</sub>O were observed with some of the oxide cations at the flows of N<sub>2</sub>O that were employed. The MO<sup>+</sup>(N<sub>2</sub>O) adduct was observed for M = Ca, Fe, Sr, Ba, Eu and Lu. Only the EuO<sup>+</sup>(N<sub>2</sub>O) adduct ion appeared to react with CO by exchanging the N<sub>2</sub>O for CO. Also observed were PtO<sub>2</sub><sup>+</sup>(N<sub>2</sub>O) and BaO<sup>+</sup>(N<sub>2</sub>O)<sub>2</sub>. The oxide cations OsO<sup>+</sup>, IrO<sup>+</sup>, and PtO<sup>+</sup> reacted further with N<sub>2</sub>O by sequential O-atom transfer to form the higher oxides OsO<sub>*n*</sub><sup>+</sup> (*n* = 2, 3, 4), IrO<sub>*n*</sub><sup>+</sup> (*n* = 2, 3), and PtO<sub>*n*</sub><sup>+</sup> (*n* = 2, 3), respectively. We can also report here a rate coefficient of 3 molecule<sup>-1</sup> s<sup>-1</sup> for the oxidation of PtO<sup>+</sup> with N<sub>2</sub>O to form PtO<sub>2</sub><sup>+</sup>.

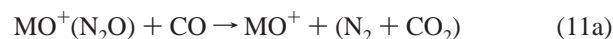
**3.3. Reduction Reactions of Metal-Monoxide Cations with CO.** Of the 16 oxide cations that could be produced by the reactions of M<sup>+</sup> cations that reacted with N<sub>2</sub>O, only 10 exhibited an observable reaction with CO: CaO<sup>+</sup>, FeO<sup>+</sup>, GeO<sup>+</sup>, SrO<sup>+</sup>, BaO<sup>+</sup>, OsO<sup>+</sup>, IrO<sup>+</sup>, PtO<sup>+</sup>, EuO<sup>+</sup>, and YbO<sup>+</sup>. Four other atomic oxide cations (CrO<sup>+</sup>, CoO<sup>+</sup>, TmO<sup>+</sup>, and LuO<sup>+</sup>) were observed not to react with CO,  $k < 10^{-13}$  cm<sup>3</sup> molecule<sup>-1</sup> s<sup>-1</sup>, and two (SeO<sup>+</sup>, ReO<sup>+</sup>) were simply too small in intensity to provide any kind of measurement.

Experimental results obtained for the 10 oxide cations that were observably reactive with CO at a fixed N<sub>2</sub>O flow are shown in Figures 1 to 3. The solid lines represent kinetic fits to the data points. The fitting of the ion profiles was performed in several different ways depending on the nature of the ion. Where possible, the decays of reactant ions were fitted using kinetic

equations for pseudo-first-order reactions. When this was not possible due to the occurrence of reaction 8 in the reaction region we used two and three component fits originally developed for multicomponent reactions. Although this latter approach provides a fit to the data, it is quite arbitrary, usually has no real physical meaning and was not used to extract rate coefficients. However, in those cases where the observed curvature actually is due to the presence of two isomers, e.g., IrO<sub>3</sub><sup>+</sup> and CaO<sup>+</sup>-(N<sub>2</sub>O,CO<sub>2</sub>)<sub>2</sub>, the fits do have physical meaning. Where possible, the N<sub>2</sub>O flow was adjusted to establish the MO<sup>+</sup> ion as the predominant ion before CO addition. This was not achieved with YbO<sup>+</sup> because of the slow reaction of Yb<sup>+</sup> with N<sub>2</sub>O and with OsO<sup>+</sup>, IrO<sup>+</sup>, and PtO<sup>+</sup> because of their fast reactions with N<sub>2</sub>O to form higher oxide cations. With EuO<sup>+</sup> the N<sub>2</sub>O flow needed to be reduced to maximize the decay of EuO<sup>+</sup> because of its relatively slow reduction with CO (reaction 8 is much faster than reaction 9). The limits to the rate coefficients for the reduction reactions that could be determined from the initial slopes of the curved decays observed for MO<sup>+</sup> are included in Table 1.

### 3.3.1. Alkaline-Earth Oxide Cations: CaO<sup>+</sup>, SrO<sup>+</sup>, BaO<sup>+</sup>.

The reductions of CaO<sup>+</sup>, SrO<sup>+</sup>, and BaO<sup>+</sup> with CO according to reaction 9 are clearly evident in Figure 1. In the special case of CaO<sup>+</sup>, overlap in the ion signal was observed with C<sub>2</sub>O<sub>2</sub><sup>+</sup> produced by the reaction of CO with CO<sup>+</sup> produced by chemistry initiated by Ar<sup>+</sup> that could not be separated from Ca<sup>+</sup> with the upstream quadrupole. The N<sub>2</sub>O adducts of CaO<sup>+</sup>, SrO<sup>+</sup>, and BaO<sup>+</sup> formed upstream of the reaction region at the flows of N<sub>2</sub>O used in these experiments all showed reactivity with CO. Two product channels come into question, and these are shown in reaction 11.



Channel 11a can be viewed as a neutral reaction between N<sub>2</sub>O and CO driven by the bond activation of N<sub>2</sub>O by CaO<sup>+</sup>. Such bond-activation reactions have been reported previously.<sup>19,20</sup>

A more exothermic variant of reaction 11a is reaction 12 in which CO<sub>2</sub> remains attached to MO<sup>+</sup>. Here the ionic product is isobaric with the ionic reactant.



Channel 11b corresponds to an O-atom transfer in which N<sub>2</sub>O is liberated. Both channels are exothermic. Channel 11a is exothermic by the exothermicity of the neutral reaction, N<sub>2</sub>O + CO → N<sub>2</sub> + CO<sub>2</sub>, less  $D(\text{MO}^+ - \text{N}_2\text{O})$ , viz.  $\Delta H(11a) = -80$  kcal mol<sup>-1</sup> +  $D(\text{MO}^+ - \text{N}_2\text{O})$ . For channel 11b,  $\Delta H(11b) = \text{OA}(\text{M}^+) - \text{OA}(\text{CO}) + D(\text{MO}^+ - \text{N}_2\text{O})$ . Since  $\text{OA}(\text{M}^+) - \text{OA}(\text{CO}) = -50, -56, \text{ and } -34$  kcal mol<sup>-1</sup> for M<sup>+</sup> = Ca<sup>+</sup>, Sr<sup>+</sup>, and Ba<sup>+</sup>, respectively, channel 11a is more exothermic than channel 11b. Our experiments indicate that channels 11a and 12 occur for M = Ca: a definite rise in the CaO<sup>+</sup> signal was associated with the disappearance of CaO<sup>+</sup>(N<sub>2</sub>O), and a flattening in the  $m/z = 100$  signal which we attribute to

(20) Viggiano, A. A.; Deakynne, C. A.; Dale, F.; Paulson, J. F. *J. Chem. Phys.* **1987**, *87*, 6544.

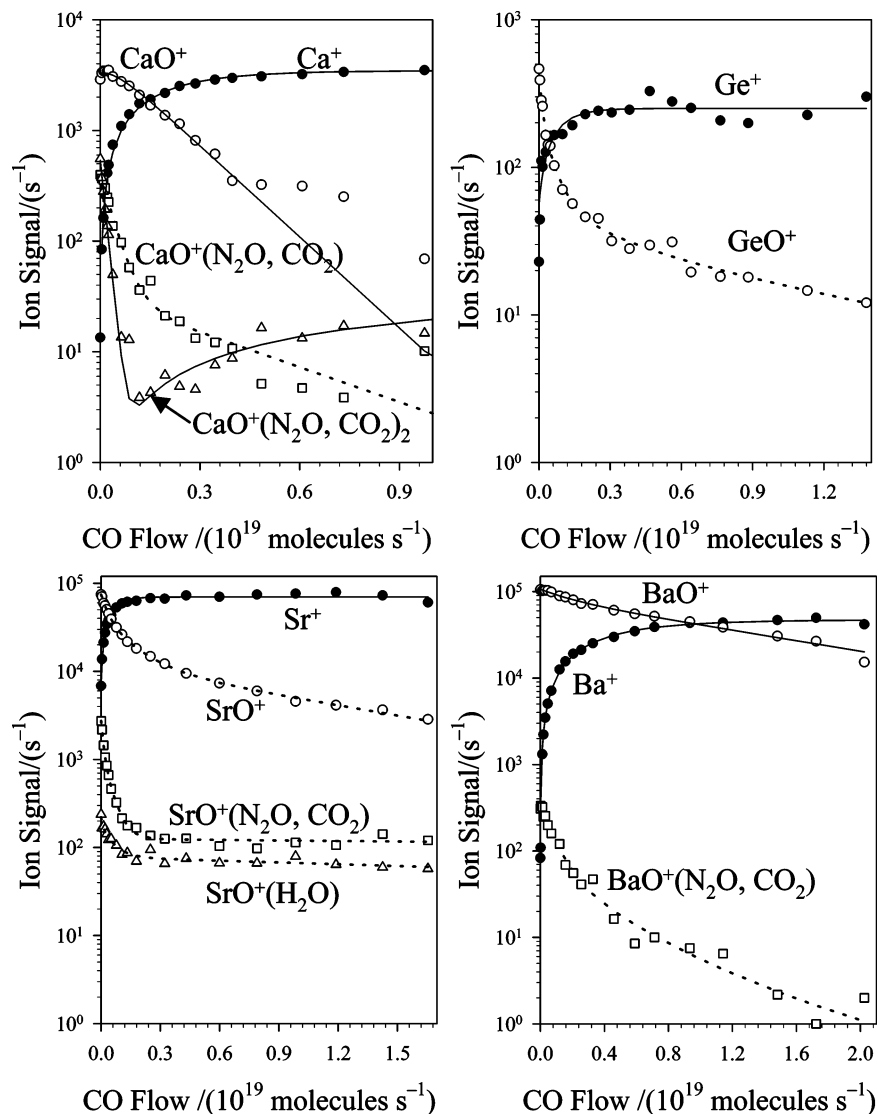
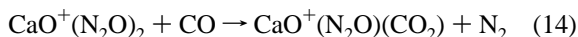
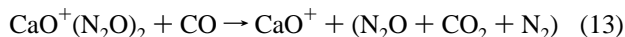
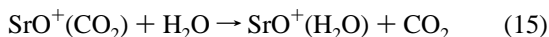


**Figure 1.** Ion profiles recorded for the chemistry initiated by  $\text{CaO}^+$ ,  $\text{GeO}^+$ ,  $\text{SrO}^+$ , and  $\text{BaO}^+$  with carbon monoxide at 295 K in helium buffer gas at 0.35 Torr. The  $\text{CaO}^+$  profile has been corrected for overlap with  $\text{C}_2\text{O}_2^+$  (see text). The flows of  $\text{N}_2\text{O}$  added upstream are 0.8, 0.2, 2, and  $1 \times 10^{18}$  molecules  $\text{s}^{-1}$ . Dashed lines are nonkinetic fits. Solid lines are kinetic fits based on the initial slopes of the decays of relevant precursor ions.

$\text{CaO}^+(\text{CO}_2)$  is seen at high flows of CO (see Figure 1). The analogues of reactions 11a and 12 involving the second  $\text{N}_2\text{O}$  adduct of  $\text{CaO}^+$ , viz. reactions 13 and 14,



also appear to occur; this time an ion with the mass of  $\text{CaO}^+(\text{N}_2\text{O})(\text{CO}_2)$  that can be produced by reaction 14 shows a definite increase at higher CO flows (see Figure 1). Reactions 11a and 12 also appear to occur for  $\text{M} = \text{Sr}$ : we attribute the flattening in the  $m/z = 148$  signal to the formation of  $\text{SrO}^+(\text{CO}_2)$  at high flows of CO. Also, it appears that this ion can exchange ligands according to reaction 15



with the water impurity in the buffer gas. In comparison, reaction 12 appears to contribute little, if at all, to a formation of  $m/z = 198$  ( $\text{BaO}^+(\text{CO}_2)$ ) at high flows of CO. We attribute the loss of

the ion at  $m/z = 198$  to the analogue of reaction 11a, but we cannot exclude the occurrence of the analogue of reaction 12.

**3.3.2.  $\text{GeO}^+$ .** The measurements for the reaction of  $\text{GeO}^+$  with CO were simplified by the absence of  $\text{N}_2\text{O}$  adduct ions. As shown in Figure 1, only  $\text{Ge}^+$  was observed as a product ion that was formed by reaction 9 ( $\text{M} = \text{Ge}$ ) with  $k \geq 1.1 \times 10^{-10}$   $\text{cm}^3 \text{ molecule}^{-1} \text{ s}^{-1}$ .

**3.3.3.  $\text{FeO}^+$ .** Figure 2 shows ion profiles for the reaction of  $\text{FeO}^+$  with CO, reaction 5. Experiments at low flows of  $\text{N}_2\text{O}$  indicate a lower limit of  $k \geq 2.4 \times 10^{-10}$   $\text{cm}^3 \text{ molecule}^{-1} \text{ s}^{-1}$  for this reaction. This value is in agreement with our earlier SIFT value of  $k = 2.05(\pm 30\%) \times 10^{-10}$   $\text{cm}^3 \text{ molecule}^{-1} \text{ s}^{-1}$  determined from experiments in which  $\text{FeO}^+$  was produced from a 1% mixture of  $\text{Fe}(\text{CO})_5$  in  $\text{N}_2\text{O}$  in an electron-impact ion source.<sup>3</sup>

$\text{FeO}^+$  readily adds  $\text{N}_2\text{O}$  in a sequential fashion,<sup>3</sup> and this accounts for the initial presence of  $\text{FeO}^+(\text{N}_2\text{O})_{1,2,3}$  in the reaction profiles shown in Figure 2. Careful inspection of the profiles of  $\text{FeO}^+(\text{N}_2\text{O})_{1,2,3}$  at very low flows of CO clearly indicates

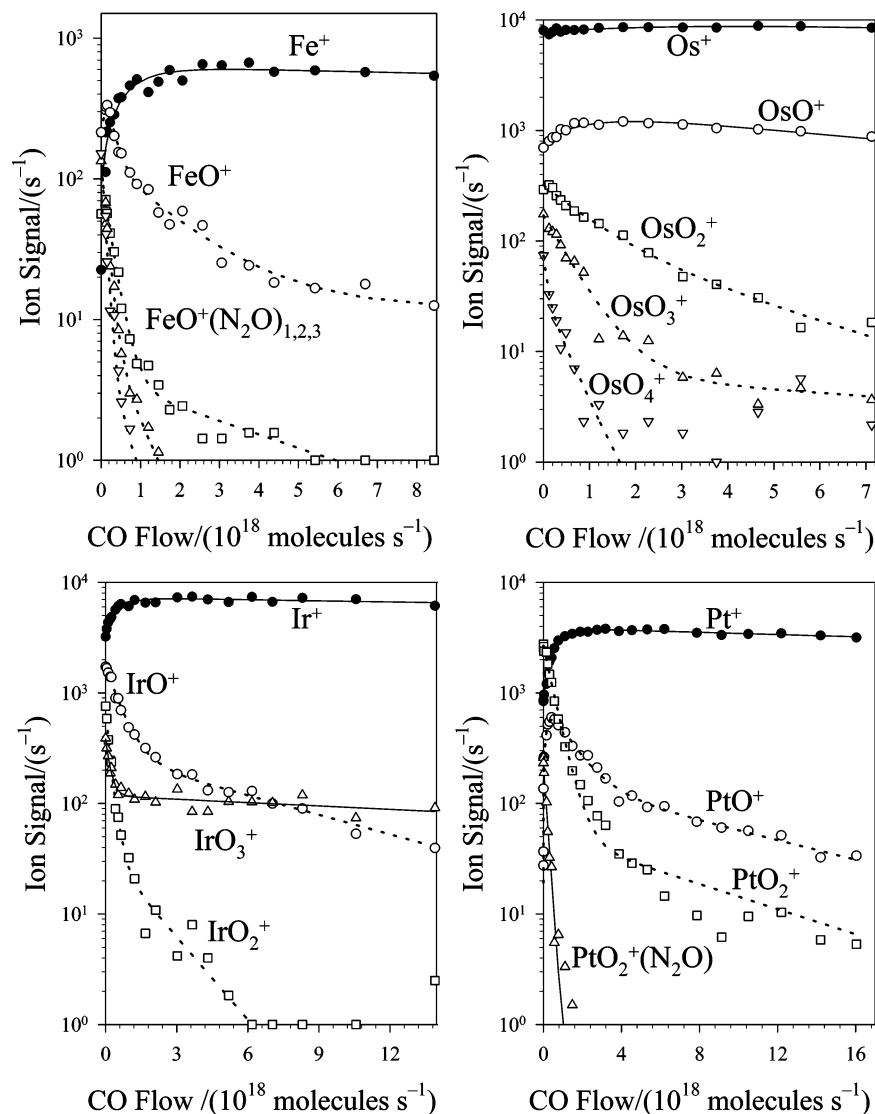
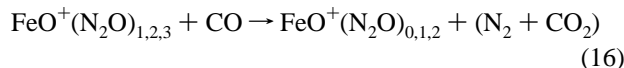
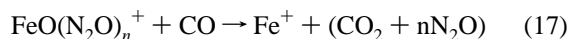


**Figure 2.** Ion profiles recorded for the chemistry initiated by  $\text{FeO}^+$ ,  $\text{OsO}^+$ ,  $\text{IrO}^+$ , and  $\text{PtO}^+$  with carbon monoxide at 295 K in helium buffer gas at 0.35 Torr. The flows of  $\text{N}_2\text{O}$  added upstream are 2.5, 0.03, 0.2, and  $0.4 \times 10^{18}$  molecules  $\text{s}^{-1}$ . Dashed lines are nonkinetic fits. Solid lines are kinetic fits based on the initial slopes of the decays of relevant precursor ions.

the production of  $\text{FeO}^+$  and  $\text{FeO}^+(\text{N}_2\text{O})$ , and by analogy  $\text{FeO}^+(\text{N}_2\text{O})_2$ , by reaction 16.



The disappearance of these ions had previously been attributed to reaction 17.

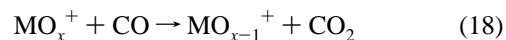


The conditions of the latter experiments were not varied sufficiently to discern the production of  $\text{FeO}^+(\text{N}_2\text{O})_{0,1,2}$  by reaction 16.

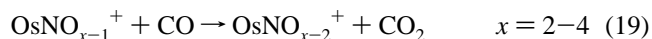
**3.3.4.  $\text{OsO}^+$ ,  $\text{IrO}^+$ ,  $\text{PtO}^+$ .** The profiles shown in Figure 2 for the reactions of the oxide cations of the platinum-group elements Os, Ir, and Pt all show similar chemistry. The initial slopes for the semilogarithmic decays of the oxide cations indicate limits of  $\geq 4.6 \times 10^{-11}$ ,  $\geq 2.6 \times 10^{-11}$ , and  $\geq 1.2 \times 10^{-10}$   $\text{cm}^3 \text{ molecule}^{-1} \text{ s}^{-1}$  for the rate coefficients for reaction 9 with  $\text{M} = \text{Os}$ ,  $\text{Ir}$ , and  $\text{Pt}$ , respectively. Analysis of the  $\text{OsO}^+$

profile was complicated because of  $\text{OsN}^+$  production (60%) in the reaction of  $\text{Os}^+$  with  $\text{N}_2\text{O}$ <sup>5,8</sup> and some overlap between  $\text{OsN}^+$  and  $\text{OsO}^+$ . However,  $\text{OsN}^+$  appeared to be unreactive with CO so that the overlap could be corrected for.

Higher-order  $\text{N}_2\text{O}$  chemistry with  $\text{OsO}^+$ ,  $\text{IrO}^+$ , and  $\text{PtO}^+$  leads to formation of higher oxide cations according to reaction 18 with  $\text{M} = \text{Os}$  ( $x = 1-4$ ),  $\text{Ir}$  ( $x = 1-3$ ), and  $\text{Pt}$  ( $x = 1-3$ ).<sup>5,8</sup>



The results with Os again were more complicated, in this case by the partial overlap of  $\text{OsO}_x^+$  with  $\text{OsNO}_{x-1}^+$  formed by the sequential oxidation of  $\text{OsN}^+$  by  $\text{N}_2\text{O}$ .<sup>8</sup> The  $\text{OsNO}_{x-1}^+$  ions appeared to be reduced by CO according to reaction 19.



The ion with  $m/z$  corresponding to  $\text{IrO}_3^+$  showed unusual behavior in that about 10% of this ion appeared not to react. It is possible that  $\text{IrO}_3^+$  formed by the reaction of  $\text{IrO}_2^+$  with  $\text{N}_2\text{O}$  is produced in two isomeric forms, one involving three  $\text{Ir}^+-\text{O}$

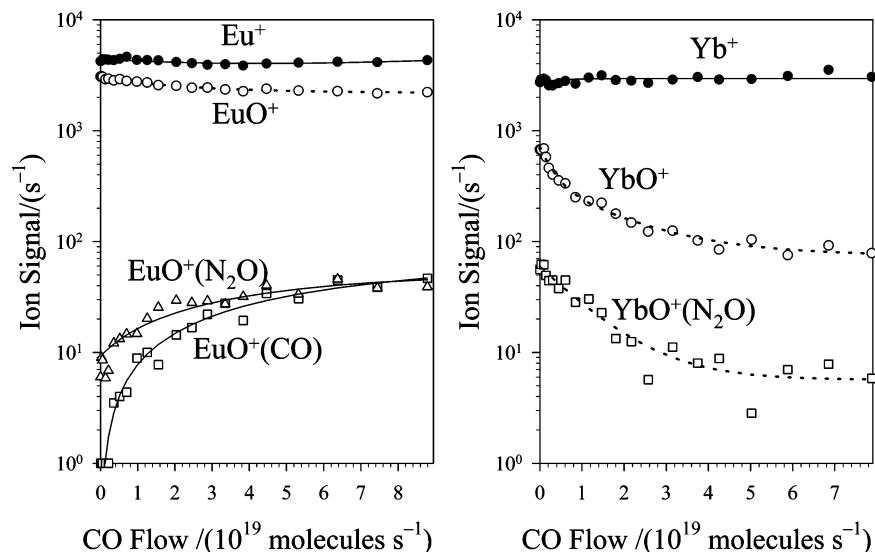
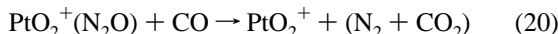


**Figure 3.** Ion profiles recorded for the chemistry initiated by  $\text{EuO}^+$  and  $\text{YbO}^+$  with carbon monoxide at 295 K in helium buffer gas at 0.35 Torr. The flows of  $\text{N}_2\text{O}$  added upstream are  $3$  and  $4 \times 10^{17}$  molecules  $\text{s}^{-1}$ . The initial slopes in the decays of  $\text{MO}^+$  were used to fit the formation of product ions (solid lines).

bonds and the second one with an O—O bond and superoxide-like structure ( $\text{O}=\text{Ir}^+-\text{O}-\text{O}$ ). Due to the difference in binding, one of the isomers would be quickly reduced by CO, while the reduction of the other isomer would proceed much slower, possibly due to presence of an activation barrier. However, in principle, we cannot rule out the initial formation of some hot or electronically excited ions of one structure from the reaction of  $\text{IrO}_2^+$  with  $\text{N}_2\text{O}$ . The rapid disappearance with CO addition of the observed adduct ion  $\text{PtO}_2^+(\text{N}_2\text{O})$  is attributed to reaction 20 which is analogous to reaction 16.



**3.3.5. Lanthanum Oxide Cations:  $\text{EuO}^+$ ,  $\text{YbO}^+$ .** The lanthanide cations  $\text{Eu}^+$  and  $\text{Yb}^+$  are borderline catalysts from the kinetic point of view (see Figure 3): they abstract an O atom from  $\text{N}_2\text{O}$  only very slowly, particularly  $\text{Yb}^+$ , because of the relatively large energy required to promote one electron from the  $4f^7 5d^0 6s^1$  to the  $4f^8 5d^1 6s^1$  configuration and so to make two electrons available for bonding with O.<sup>21</sup> The reduction of the oxide cations with CO also appears slow, although only lower limits to the rate coefficients could be obtained (see Table 1). The reduction of  $\text{EuO}^+$  competes with addition of CO (<20% at the He pressure of our experiments), as some formation of  $\text{EuO}^+(\text{CO})$  was observed.  $\text{EuO}^+(\text{CO})$  may undergo a switching reaction with  $\text{N}_2\text{O}$  to produce the concomitant rise in  $\text{EuO}^+(\text{N}_2\text{O})$ . Alternatively,  $\text{EuO}^+(\text{N}_2\text{O})$  may be produced directly in a termolecular reaction of type 21 with CO acting as the third body.



$\text{N}_2\text{O}$  addition to  $\text{YbO}^+$  appears to poison the catalysis as  $\text{YbO}^+(\text{N}_2\text{O})$  appears not to be reduced by CO; the  $\text{YbO}^+(\text{N}_2\text{O})$  signal declines in response to the decline in the precursor ion instead (see Figure 3).

**3.4. Catalytic Cycles and Steady State.** For O-atom transport catalysis to be effective, both legs of the catalytic cycle, given by reactions 8 and 9 and shown in Scheme 1, must be rapid.

Both of these reactions occur in the reaction region of the flow tube with the  $10 \text{ MO}^+$  ions that were observed to produce  $\text{M}^+$  by reaction with CO because of the presence of  $\text{N}_2\text{O}$  added upstream to produce  $\text{MO}^+$  from  $\text{M}^+$ . Consequently the catalytic cycle shown in Scheme 1 can be expected to achieve steady state within the reaction region, since the half-lives of the oxidation and reduction reactions ( $<10^{-5}$  s) are much shorter than the total reaction time (ca. 5 ms). The steady state was monitored with plots of  $[\text{M}^+]/[\text{MO}^+]$  versus CO flow, since  $d[\text{M}^+]/dt = d[\text{MO}^+]/dt = 0$ , and as a consequence,  $[\text{M}^+]/[\text{MO}^+] = k_9[\text{CO}]/(k_8[\text{N}_2\text{O}])$  at steady state. Families of such plots are shown in Figure 4 for  $\text{M}^+/\text{MO}^+ = \text{Fe}^+/\text{FeO}^+$ ,  $\text{Ge}^+/\text{GeO}^+$ ,  $\text{Pt}^+/\text{PtO}^+$ , and  $\text{PtO}^+/\text{PtO}_2^+$ , each at three different flows of  $\text{N}_2\text{O}$ . It is perhaps surprising at first glance that no effects are seen of the approach to steady state at low CO flows, but this is consistent with the relative magnitude of the half-lives of the oxidation and reduction reactions ( $<10^{-5}$  s) and the total reaction time (ca. 5 ms).

The observed linearity in these plots is indicative of the attainment of steady state and provides a measure of  $k_8/k_9$  when the flow of  $\text{N}_2\text{O}$  is known. Table 2 provides a summary of the values of  $k_8/k_9$  determined from the observed linearities in plots of  $[\text{M}^+]/[\text{MO}^+]$  vs CO flow. Knowledge of  $k_8/k_9$  allows the determination of  $k_9$  when  $k_8$  is measured independently in the absence of CO as we have done for the systems investigated here. Table 3 provides average values of  $k_8/k_9$ , and values of  $k_9$  determined in this fashion are included in Table 1. In the case of  $\text{Pt}^+/\text{PtO}^+$  and  $\text{PtO}^+/\text{PtO}_2^+$  a slight dependence was observed for  $k_8/k_9$  on the  $\text{N}_2\text{O}$  flow (see Table 2). This is attributed to the reduction of the respective higher-order species ( $\text{PtO}_2^+$  and  $\text{PtO}_3^+/\text{PtO}_2^+\cdot\text{N}_2\text{O}$ ) which provide an increasing source for  $\text{PtO}^+$  and  $\text{PtO}_2^+$  with  $\text{N}_2\text{O}$  flow. The values of  $k_8/k_9$  reported for  $\text{Pt}^+/\text{PtO}^+$  (0.53) and  $\text{PtO}^+/\text{PtO}_2^+$  (2.6) are those obtained by extrapolation to zero  $\text{N}_2\text{O}$  flow. Higher oxides were not observed with  $\text{Ca}^+$  and  $\text{Ba}^+$ , and their monoxide clusters were too small to provide a significant source of the monoxide cations. This means that the scatter in the values for  $k_8/k_9$  shown in Table 2 in these two cases is a measure of experimental uncertainty.

Generally speaking, the reduction of  $\text{N}_2\text{O}$  by  $\text{M}^+$  that occurs in the reaction region can be sufficiently exothermic to leave

(21) Koyanagi, G. K.; Bohme, D. K. *J. Phys. Chem. A* **2001**, *103*, 8964.



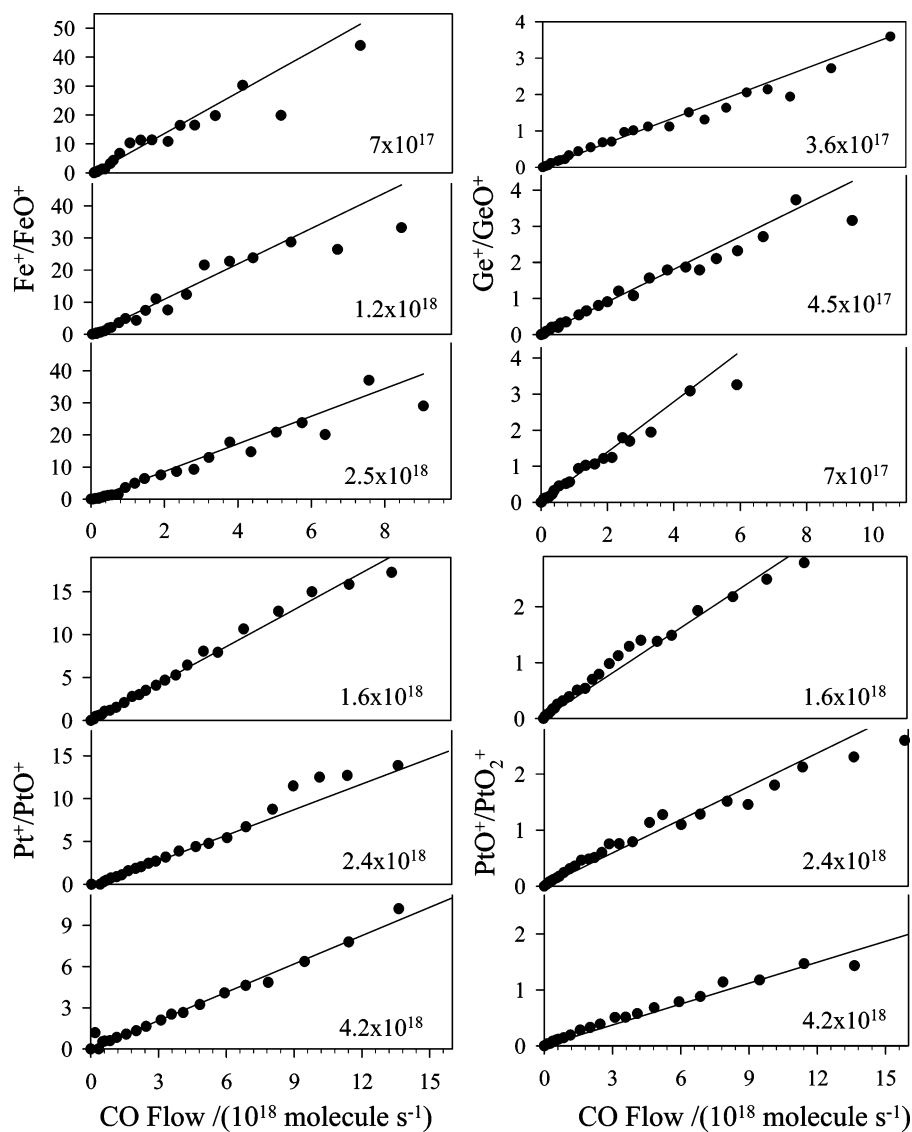


**Figure 4.** Plots demonstrating the attainment of steady state for the catalytic cycles involving  $\text{Fe}^+$  (top left),  $\text{Ge}^+$  (top right),  $\text{Pt}^+$  (bottom left), and  $\text{PtO}^+$  (bottom right) at various flows of  $\text{N}_2\text{O}$  given in the bottom right-hand corner in units of molecules  $\text{s}^{-1}$ .

$\text{MO}^+$  with some internal excitation. This internal excitation may not be sufficiently quenched by the number of collisions with He buffer gas and  $\text{N}_2\text{O}$  to be thermalized before reacting with CO. Similarly, the  $\text{M}^+$  produced in the oxidation of  $\text{MO}^+$  by CO may be produced with some internal and kinetic excitation that may not be sufficiently quenched by the number of collisions with He buffer gas and added CO to be thermalized before reacting with  $\text{N}_2\text{O}$ ; viz. the catalysis may be proceeding under nonthermalized conditions. However, this appears not to be the case in the experiments reported here at the operating conditions in the reaction region of the flow tube in which He is in large excess. Within the uncertainty of the measurements, the values obtained for  $k_8/k_9$  appear to be independent of the  $\text{N}_2\text{O}$  flow (or nearly so for  $\text{Pt}^+$  and  $\text{PtO}^+$ ), and the plots appear linear over the entire range of CO flow. Generally speaking, this can be expected to be the case in the presence of a buffer gas in sufficiently large excess to ensure thermalization and of course also when  $k_8$  and  $k_9$  are insensitive to internal excitation. Also, the  $\text{N}_2\text{O}$  and CO dependence will be minimal for catalytic couples in which the excitation of ions produced in the individual steps is minimal. For the metal cations

investigated here that lie within the thermodynamic window, a low exothermicity in one of the two steps will mean high exothermicity in the other step, since  $\Delta H_1 + \Delta H_2 = \text{OA}(\text{N}_2\text{O}) - \text{OA}(\text{CO})$ . In the case of the  $\text{Fe}^+/\text{FeO}^+$  cycle, the presence of thermalization can be further tested, since both  $k_8$  and  $k_9$  have been measured independently with thermalized ions. The value for  $k_9 = 2.4(\pm 40\%) \times 10^{-10} \text{ cm}^3 \text{ molecule}^{-1} \text{ s}^{-1}$  derived here from  $k_9/k_8$  agrees, within experimental error, with the value of  $2.05(\pm 30\%) \times 10^{-10} \text{ cm}^3 \text{ molecule}^{-1} \text{ s}^{-1}$  reported earlier in an independent study of the reaction of  $\text{FeO}^+$  thermalized upstream of the flow tube with CO added to the reaction region.<sup>3</sup>

The observed reduction of higher oxide cations of Os, Ir, and Pt according to reaction 18 and their formation by oxidation with  $\text{N}_2\text{O}$  as described previously<sup>8</sup> define coupled catalytic cycles as the one shown for Os in Scheme 2 which leads to the reduction of  $\text{N}_2\text{O}$  by CO. The rapid disappearance of the higher oxide cations prevented the evaluation of  $k_{\text{ox}}/k_{\text{red}}$  in these cases. The one exception is the  $\text{PtO}^+/\text{PtO}_2^+$  cycle for which we were able to determine  $k_{\text{ox}}/k_{\text{red}} = 2.6$ .

Also, the observed occurrence of reactions of  $\text{N}_2\text{O}$  adduct ions with CO of type 14a with  $\text{M} = \text{Fe}$  and  $\text{Pt}$  involving  $\text{N}_2\text{O}$

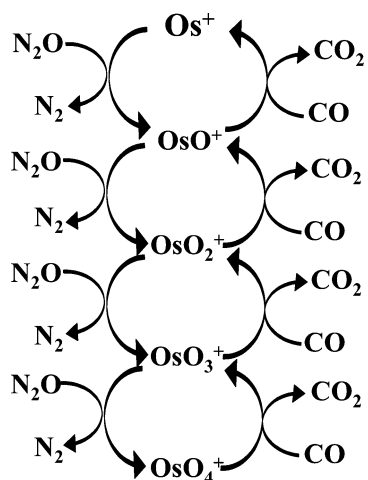
**Table 2.** Summary of Measurements of  $k_8/k_9$  at Different Flows of  $N_2O$ 

catalytic ions	$N_2O$ flow (molecules $s^{-1}$ )	$k_8/k_9$
$Ca^+/CaO^+$	$1.3 \times 10^{18}$	0.56
$Ca^+/CaO^+$	$2.5 \times 10^{18}$	0.79
$Fe^+/FeO^+$	$0.3 \times 10^{18}$	0.22
$Fe^+/FeO^+$	$0.7 \times 10^{18}$	0.21
$Fe^+/FeO^+$	$1.3 \times 10^{18}$	0.20
$Fe^+/FeO^+$	$2.5 \times 10^{18}$	0.20
$Ge^+/GeO^+$	$0.9 \times 10^{18}$	0.17
$Ge^+/GeO^+$	$1.3 \times 10^{18}$	0.17
$Ge^+/GeO^+$	$1.8 \times 10^{18}$	0.18
$Ba^+/BaO^+$	$1.5 \times 10^{18}$	12.0
$Ba^+/BaO^+$	$2.1 \times 10^{18}$	9.1
$Pt^+/PtO^+$	$0.4 \times 10^{18}$	0.54
$Pt^+/PtO^+$	$1.7 \times 10^{18}$	0.41
$Pt^+/PtO^+$	$2.4 \times 10^{18}$	0.41
$Pt^+/PtO^+$	$4.2 \times 10^{18}$	0.35
$PtO^+/PtO_2^+$	$0.4 \times 10^{18}$	2.6
$PtO^+/PtO_2^+$	$1.7 \times 10^{18}$	2.0
$PtO^+/PtO_2^+$	$2.4 \times 10^{18}$	1.8
$PtO^+/PtO_2^+$	$4.2 \times 10^{18}$	1.5

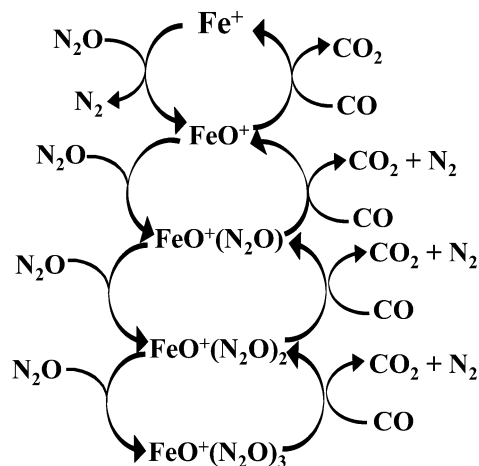
**Table 3.** Values for  $k_8/k_9$  Obtained from the Steady-State Analysis (see Table 2)<sup>a</sup>

catalytic ions	$k_8/k_9^b$	$E_{ox}^c$	$E_{red}^c$	$E_{cycle}^d$
$Ca^+/CaO^+$	0.70	0.17	0.32	0.054
$Fe^+/FeO^+$	0.21	0.043	0.24	0.010
$Ge^+/GeO^+$	0.17	0.44	0.28	0.12
$Sr^+/SrO^+$	0.63	0.080	0.14	0.011
$Ba^+/BaO^+$	10.6	0.32	0.033	0.011
$Os^+/OsO^+$	180 <sup>e</sup>	0.082	NA	NA
$Ir^+/IrO^+$	0.85	0.41	0.51	0.21
$Pt^+/PtO^+$	0.53	0.17	0.34	0.058
$Eu^+/EuO^+$	NA	0.097	NA	NA
$Yb^+/YbO^+$	0.06	$9.3 \times 10^{-4}$	0.018	$1.7 \times 10^{-5}$
$PtO^+/PtO_2^+$	2.6	0.82	0.32	0.26

<sup>a</sup> Also included are the reaction efficiencies for the oxidation and reduction steps and the efficiency of the complete catalytic cycle all at 295 K (see text). <sup>b</sup> The uncertainties represent the precision of the measurements. Unless indicated otherwise, the estimated accuracy is  $\pm 20\%$ . NA indicates that the required rate coefficients were not available. <sup>c</sup>  $E_{ox}$  and  $E_{red}$  are equal to the ratio of the reaction-rate coefficient to the collision-rate coefficient,  $(k/k_c)$  and  $(k/k_{c_0})$ , respectively. <sup>d</sup> The absolute accuracy in the value of  $E_{cycle}$  is estimated to be less than 60%. <sup>e</sup> This value should be regarded as an upper limit because of overlap of  $OsO^+$  with unreactive  $OsN^+$ .

**Scheme 2**

adduct ions and their formation by addition to the metal oxide cation<sup>8</sup> define coupled catalytic cycles as the one shown for Fe in Scheme 3 which also leads to the reduction of  $N_2O$  by CO.

**Scheme 3**

The rapid disappearance of these adducts again prevented a steady-state analysis.

**3.5. Potential Energy Landscape for Catalysis.** The potential-energy landscape computed for the reduction of  $N_2O$  by CO catalyzed by  $Fe^+$  (<sup>6</sup>D) according to reactions 1 to 3 is shown in Figure 5. All the intermediates and transition state structures on the catalyzed pathway are in the sextet electronic state. The uncatalyzed reduction shown in the top profile proceeds in one step via a high activation barrier of 47.2 kcal mol<sup>-1</sup> and is strongly exothermic, by 86.7 kcal mol<sup>-1</sup> according to the calculations and by 87 kcal mol<sup>-1</sup> according to published enthalpies of formation.<sup>6</sup> The structure of the transition state corresponds to a direct attack of oxygen atom of  $N_2O$  on the carbon atom of CO. The N–O bond is being broken, and the C–O bond is being formed. The activation barrier for the uncatalyzed reduction of  $N_2O$  by CO, apparently due to the cleavage of the N–O bond, is lowered by more than a factor

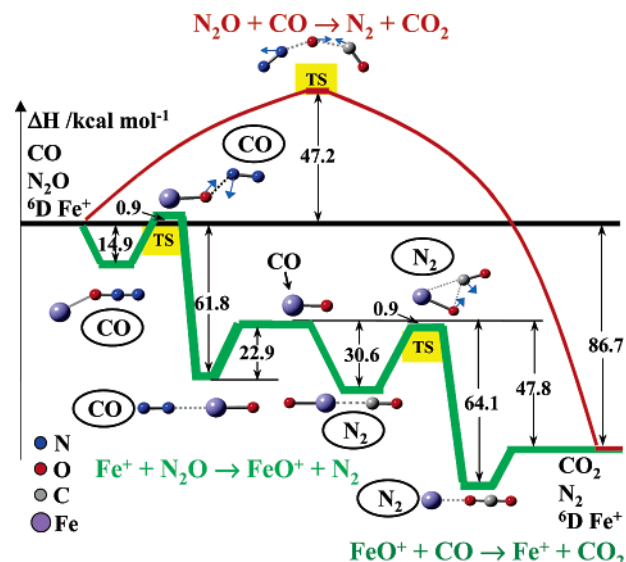


**Figure 5.** Energy landscape for the reduction of  $N_2O$  by CO in the absence and presence of  $Fe^+$  (<sup>6</sup>D) computed using DFT with hybrid B3LYP exchange-correlation functional and a triply split 6-311+G(d) basis set with one set of diffuse and polarization functions. The red profile corresponds to the neutral reaction of  $N_2O$  with CO. The green profiles correspond to the linked catalytic ion–molecule reactions of  $Fe^+$  with  $N_2O$  and of  $FeO^+$  with CO. The bold black line corresponds to the dissociation limit to  $Fe^+$ ,  $N_2O$ , and CO. Spectator molecules are indicated in ovals. Transition state structures are labeled with TS; transition state vectors are sketched.

of 50 to a mere 0.9 kcal mol<sup>-1</sup> that arises in the first step of the much faster ionic path. The reaction coordinates of both ionic steps in this path are described by double-minimum potential-energy profiles. The first step involves O-atom transfer from N<sub>2</sub>O to Fe<sup>+</sup> with the formation of FeO<sup>+</sup> and N<sub>2</sub>. The activation barrier is 0.9 kcal mol<sup>-1</sup> above the dissociation limit. This is somewhat lower than the barrier of 4.2 kcal mol<sup>-1</sup> that we predicted recently using the B3LYP/sdd/6-311+G(d) method with the relativistic ECP and a double- $\zeta$  basis set for iron.<sup>8</sup> The higher value obtained might be attributable to the limitations of the ECP and basis set that was used. The second step in the catalyzed reduction of N<sub>2</sub>O by CO involves O-atom transfer from FeO<sup>+</sup> to CO with the formation of Fe<sup>+</sup> and CO<sub>2</sub> and proceeds without a barrier. The energy of the transition state in the second step lies 0.9 kcal mol<sup>-1</sup> below the dissociation limit to FeO<sup>+</sup> and CO.

The catalysis in the reaction region of the flow tube proceeds in a helium bath at a pressure of 0.35 Torr so that any excess energy that appears in FeO<sup>+</sup> produced in the first step of the catalysis is relaxed by many collisions with He atoms before FeO<sup>+</sup> collides with CO and can complete the catalysis.

**3.6. Efficiency of Catalysis.** The so-called “turnover number”,  $N$ , defined as the number of molecules converted by one catalytic ion, is often used as a numerical measure of the efficiency of catalysis. Numerically it is given by the expression  $N = \phi/(1 - \phi)$  where  $\phi$  is the fraction of the catalytic channel in the reaction cycle ( $\phi = \phi_1\phi_2$  if each leg of the cycle is fractionally depleted by competing channels). When the only channel is the catalytic channel, viz. in the absence of any competing channels, as is the case in Scheme 1, and for all but two of the 10 atomic catalytic redox couples observed in this study,  $\phi$  is  $> 0.99$  and  $N$  is  $> 99$ . The “intrinsic” turnover number defined in this way therefore is not very useful for distinguishing the relative merits of these catalytic cations. Os<sup>+</sup> is an exception because of OsN<sup>+</sup> formation and Eu<sup>+</sup> because EuO<sup>+</sup> clusters with CO; both competing channels act to reduce the turnover number. To be sure, in a real chemical system, the intrinsic turnover number would be modified (reduced) by the presence of gases that react with M<sup>+</sup> or MO<sup>+</sup> in another fashion and so compete with the catalytic cycle.

We propose here, for the first time, a measure of the intrinsic efficiency,  $E_{\text{cycle}}$ , for individual catalytic cycles in order to allow a quantitative measure of the relative intrinsic merits of catalytic cations *in the absence of competing reaction channels*. We explicitly take into account the reaction efficiency of each of the two legs of such cycles and so define  $E_{\text{cycle}}$  as shown in eq 22

$$\text{Efficiency, } E_{\text{cycle}} = E_{\text{ox}} \times E_{\text{red}} = (k/k_c)_8 \times (k/k_c)_9 \quad (22)$$

in terms of the product of the reaction efficiency,  $E = k/k_c$ , for each of the two component reactions of the catalytic cycle, the oxidation reaction 8 and the reduction reaction 9 in our case. According to this definition the efficiency  $E_{\text{cycle}}$  has a maximum value of 1 (or 100%). Perhaps we should emphasize that  $E_{\text{cycle}}$  defined in this way, on a per cycle basis, does not replace the turnover number as a measure of the overall efficiency of catalysis which becomes useful in the presence of competing reaction channels. However, the definition of  $E_{\text{cycle}}$  also could be extended to take into account competing reaction channels by multiplying  $E_{\text{ox}}$  by  $\phi_{\text{ox}}$  and  $E_{\text{red}}$  by  $\phi_{\text{red}}$ , but this approach

still should be restricted to a measure of  $E_{\text{cycle}}$  for individual catalytic cycles.

If a temperature is to be ascribed to  $E_{\text{cycle}}$ , then it is necessary that the measured reaction-rate coefficients correspond to thermalized conditions at a known temperature. Otherwise the measured efficiency becomes an instrumental artifact. In the absence of thermalization the instrumental efficiency will be influenced by the partitioning of the excess energy of the oxidation and reduction reactions and so perhaps on the position of OA(M<sup>+</sup>) in the thermodynamic window for O-atom transport. Of course any kinetic barriers that influence the magnitude of the reaction-rate coefficients for oxidation and reduction will influence the magnitude of  $E_{\text{cycle}}$ . Since N<sub>2</sub>O and CO<sub>2</sub> and N<sub>2</sub> and CO are isoelectronic with the same spin configuration, any spin constraints in one step would be a constraint in the other step in the catalysis and lead to lower values for  $E_{\text{cycle}}$ , although details of the crossings of the spin surfaces may differ.

The experimental rate coefficients used in the calculation of the efficiencies,  $E_{\text{cycle}}$ , for the catalytic cycles reported here were as follows. The values for  $k_8$  were taken from measurements reported previously in which the atomic ions were generated in the same ICP source as used here and in which N<sub>2</sub>O was added into the reaction region downstream of the flow tube (in the absence of CO).<sup>8</sup> Even though the catalytic cations produced within the ICP have substantial excited-state populations at their point of origin, there were no indications of excited-state effects in these measurements of  $k_8$ .<sup>8</sup> The values for  $k_9$  used in the calculation of  $E_{\text{cycle}}$  were derived from the steady-state analyses presented above which provide a measure of  $k_8/k_9$  as already indicated.

Efficiencies computed according to eq 22 for the catalytic atomic cations identified in our study are included in Table 3 where they are seen to range from  $1.7 \times 10^{-5}$  (for Yb<sup>+</sup>/YbO<sup>+</sup>) to 0.21 (for Ir<sup>+</sup>/IrO<sup>+</sup>). They indicate the following order of efficiency: Ir<sup>+</sup>/IrO<sup>+</sup> (0.21) > Ge<sup>+</sup>/GeO<sup>+</sup> (0.12) > Pt<sup>+</sup>/PtO<sup>+</sup> (0.058) = Ca<sup>+</sup>/CaO<sup>+</sup> (0.054) > Sr<sup>+</sup>/SrO<sup>+</sup> (0.011) = Ba<sup>+</sup>/BaO<sup>+</sup> (0.011) = Fe<sup>+</sup>/FeO<sup>+</sup> (0.010) > Yb<sup>+</sup>/YbO<sup>+</sup> ( $1.7 \times 10^{-5}$ ). The positions of the 10 M<sup>+</sup> cations identified as catalysts on the periodic table are indicated in Figure 6. Also included in Table 3 is the efficiency (0.26) of the one catalytic diatomic cation (PtO<sup>+</sup>) identified in the study. This efficiency is the highest among all the cations investigated.

The main-group metal cation Ge<sup>+</sup> (p<sup>1</sup>) has OA(Ge<sup>+</sup>) = 81.8 kcal mol<sup>-1</sup> which is about in the middle of the thermodynamic window, halfway between 40 and 127 kcal mol<sup>-1</sup>. So both legs of the catalytic cycle are equally exothermic; they have about equal efficiencies:  $E_{\text{ox}} = 0.44$  and  $E_{\text{red}} = 0.28$ . The overall efficiency for the cycle is relatively high (12%). We suspect that the known value OA(Ir<sup>+</sup>) = 59 kcal mol<sup>-1</sup> should actually be 15 kcal mol<sup>-1</sup> higher based on our observation of O-atom transfer of NO<sub>2</sub> to Ir<sup>+</sup> (d<sup>7</sup>s<sup>1</sup>).<sup>5</sup> So OA(Ir<sup>+</sup>) may also lie in the middle of the thermodynamic window for catalysis. Again, both legs have relatively high efficiencies,  $E_{\text{ox}} = 0.41$  and  $E_{\text{red}} = 0.51$  and  $E_{\text{cycle}} = 21\%$ . Intermediate values are associated with  $E_{\text{cycle}}$  for Pt<sup>+</sup> (5.8%) and Ca<sup>+</sup> (5.4%) for which OA = 77 kcal mol<sup>-1</sup>. Fe<sup>+</sup> (d<sup>6</sup>s<sup>1</sup>), Sr<sup>+</sup> (s<sup>1</sup>), and Ba<sup>+</sup> (s<sup>1</sup>) all have values for  $E_{\text{cycle}}$  of about 1% at room temperature. Values for OA are 80.0, 71.4, and 92.8 kcal mol<sup>-1</sup>. Fe<sup>+</sup> and Sr<sup>+</sup> exhibit inefficient oxidation (Fe<sup>+</sup> has actually been shown to have a small kinetic barrier).<sup>8</sup> In contrast, the cycle with Ba<sup>+</sup> has an inefficient reduction step.

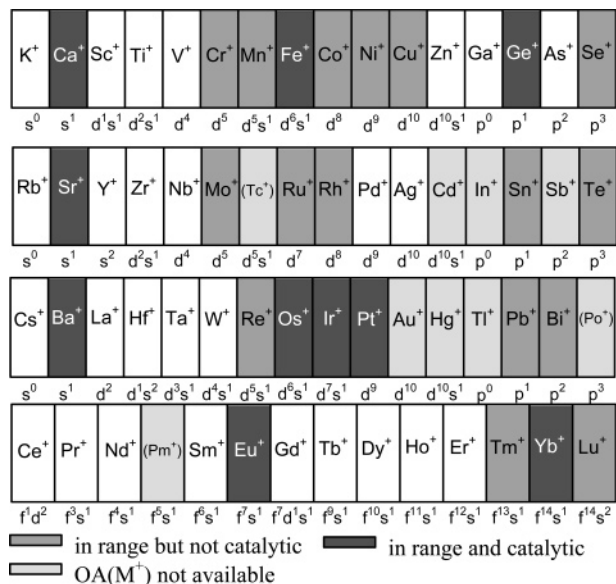


**Figure 6.** Periodic table showing atomic cations that lie in the thermodynamic window for O-atom transport catalysis of the reduction of N<sub>2</sub>O by CO and those that have been demonstrated to be catalytic.

It is interesting to note that there is a systematic decrease in  $E_{\text{red}}$  for the rare-earth cations down the periodic table from 0.32, 0.14, and 0.033 for CaO<sup>+</sup>, SrO<sup>+</sup>, and BaO<sup>+</sup>, respectively, perhaps because of increased charge delocalization with the increasing size of the metal cation. The very low cyclic efficiency for Yb<sup>+</sup> is due to the low oxidation efficiency that has been attributed to an electron-promotion energy effect.<sup>19</sup>

Our failure to measure a cyclic efficiency for the 16 other atomic cations that lie within, or perhaps just outside, the thermodynamic window for catalysis can be attributed primarily due to a low oxidation efficiency. The nonreactions involving Cr<sup>+</sup>/CrO<sup>+</sup>, Mn<sup>+</sup>/MnO<sup>+</sup>, Co<sup>+</sup>/CoO<sup>+</sup>, Ni<sup>+</sup>/NiO<sup>+</sup>, Mo<sup>+</sup>/MoO<sup>+</sup>, and Ru<sup>+</sup>/RuO<sup>+</sup> have previously been ascribed to spin constraints.<sup>8</sup> A low oxidation efficiency of course often prevented the measurement of the efficiency of reduction.

## Conclusions

The catalytic action of atomic cations in the reduction of N<sub>2</sub>O by CO has been identified as O-atom transport constrained

thermodynamically in terms of a “thermodynamic window of opportunity” some 87 kcal mol<sup>-1</sup> wide. With this window as a guide, an expanded search for atomic-cation catalysts has identified 6 new catalysts in addition to 4 that have been reported previously. The total of 10 is much less than the 26 of 59 that fall within the window. The remaining 16 potential catalysts are eliminated by kinetic constraints that arise from various causes, although 2 of these 16 potential catalysts may well lie outside this window.

Steady state was achieved in the reaction region of the ICP/SIFT tandem mass spectrometer that allowed the measurement of an efficiency for cyclic catalysis,  $E_{\text{cycle}}$ , defined here for the first time for catalytic cations *in the absence of competing reaction channels*.  $E_{\text{cycle}}$  is defined in a manner that allows it to respond to varying efficiencies for the two legs of the catalytic cycle,  $E_{\text{ox}}$  and  $E_{\text{red}}$ , and so discriminate between the performance of catalytic cycles in which competing channels are absent. This is not possible with the traditional use of the “turnover number” which would be infinite for all these cycles. Efficiencies for cyclic catalysis,  $E_{\text{cycle}}$ , are reported for eight atomic cations and one diatomic cation.

The potential-energy landscape computed for the reduction of N<sub>2</sub>O by CO catalyzed by Fe<sup>+</sup>(<sup>6</sup>D) provides a striking illustration of the operation and power of an ionic catalyst.

**Acknowledgment.** Continued financial support from the Natural Sciences and Engineering Research Council of Canada is greatly appreciated. Also, we acknowledge support from the National Research Council, the Natural Science and Engineering Research Council and MDS SCIEX in the form of a Research Partnership grant. As holder of a Canada Research Chair in Physical Chemistry, Diethard K. Bohme thanks the contributions of the Canada Research Chair Program to this research.

**Supporting Information Available:** Electronic energies and enthalpies at 0 K and Cartesian coordinates predicted for the reactions N<sub>2</sub>O + CO → N<sub>2</sub> + CO<sub>2</sub>; Fe<sup>+</sup> + N<sub>2</sub>O → FeO<sup>+</sup> + N<sub>2</sub>; and FeO<sup>+</sup> + CO → Fe<sup>+</sup> + CO<sub>2</sub> (for Figure 5) with the B3LYP/6-311+G\* method. This material is available free of charge via the Internet at <http://pubs.acs.org>.

JA044950M